Influence of interface states, conduction band offset, and front contact on the performance of a-SiC:H(n)/c-Si(p) heterojunction solar cells*

Zhi Qiao(乔治)†, Jian-Li Ji(冀建利), Yan-Li Zhang(张彦立), Hu Liu(刘虎), and Tong-Kai Li(李同锴)

Institue of Applied Physics, Department of Mathematics and Physics, Shijiazhuang Tiedao University, Shijiazhuang 050043, *China*

(Received 13 August 2016; revised manuscript received 6 January 2017; published online 20 April 2017)

P-type silicon heterojunction (SHJ) solar cells with a-SiC:H(n) emitters were studied by numerical computer simulation in this paper. The influence of interface states, conduction band offset, and front contact on the performance of a-SiC:H(n)/c-Si(p) SHJ solar cells was investigated systematically. It is shown that the open circuit voltage (V_{oc}) and fill factor (FF) are very sensitive to these parameters. In addition, by analyzing equilibrium energy band diagram and electric field distribution, the influence mechanisms that interface states, conduction band offset, and front contact impact on the carrier transport, interface recombination and cell performance were studied in detail. Finally, the optimum parameters for the a-SiC:H(n)/c-Si(p) SHJ solar cells were provided. By employing these optimum parameters, the efficiency of SHJ solar cell based on p-type c-Si was significantly improved.

Keywords: silicon heterojunction solar cells, interface states, band offset, front contact

PACS: 88.40.fc, 88.40.hj, 88.40.jj, 85.60.Bt **DOI:** 10.1088/1674-1056/26/6/068802

1. Introduction

The silicon heterojunction (SHJ) solar cell is one of the most promising candidates for photovoltaic applications due to high performance, high reliability and low cost. This type of cell features ultra-thin intrinsic and doped hydrogenated amorphous silicon (a-Si:H) layers on an n- or a p-type c-Si wafer.[1] Panasonic has achieved a record conversion efficiency of 25.6% in an SHJ structure based on n-type solar-grade c-Si.[2] It has been reported that the n-type SHJ solar cell can produce a higher efficiency because it has an inherent advantage over the p-type SHJ solar cell, due to a higher minority carrier band offset at the interface, which can result in a higher open circuit voltage.[3] In spite of this fact, the p-type c-Si wafer still dominates current industrial photovoltaics production. Moreover, the minority carrier diffusion length in p-type c-Si is higher than that in n-type material.[4] So the exploitation of SHJ solar cells on p-type c-Si is of great practical interest. In recent years, many research groups have conducted the investigation on developing high performance SHJ solar cells on p-type substrates.[5–7] So far the best efficiency of the p-type SHJ solar cell has been reached at 21.4%.[5] However, efforts are still needed to further improve the performance of the p-type SHJ solar cell.

It is well known that a very important loss mechanism of the p-type SHJ solar cells is parasitic absorption of photons in the n-type a-Si:H layer. Thus one promising way is to use a silicon-based material with wide bandgap as the window layer of the SHJ solar cell. Hydrogenated amorphous silicon carbide (a-SiC:H) with wide optical bandgap (1.8 eV–2.3 eV), low absorption in visible wavelength region, and good thermal stability is an appealing alternative for the window layer. In addition, a good interface passivation can be obtained by a high-quality a-SiC:H(n) layer.[8] Despite encouraging results having been obtained by incorporating a-SiC:H into p-type SHJ solar cells, the V_{oc} and FF are relatively low. Moreover, S-shaped I–V curves are often observed.[4,9–11] The phenomena mentioned above are closely linked to the interface states, increased heterojunction band offset and TCO/a-SiC:H front contact. A poor interface with high interface states density (D_{it}) can lead to high interface recombination. This will sharply increase dark tunneling leakage current and deteriorate V_{oc} dramatically. Considering minority carrier electrons transport across the a-SiC:H(n)/c-Si(p) heterojunction to the front contact, the minority carrier band offset (ΔE_c) and the work function of transparent conductive oxide (W_{TCO}) are of clear importance. They play crucial roles in determining the minority carriers transfer property. However, it is still a matter of debate how the D_{it}, ΔE_c, and W_{TCO} control the performance of a-SiC:H(n)/c-Si(p) SHJ solar cells. Thus we addressed this question by means of numerical computer simulation method in order to improve the performance of p-type SHJ solar cells. The purpose of this work is to systematically study the influence mechanisms of these parameters.

In this paper, the SHJ solar cells with the structure of TCO/a-SiC:H(n)/c-Si(p) (textured)/a-Si:H(i)/a-Si:H(p+)/TCO were modeled by using AFORS-HET software. We discussed in detail the influence of the interface states density, conduction band offset and front contact work function on the pho-

*Project supported by the National High Technology Research and Development Program of China (Grant No. 2012AA050301) and Scientific Research of Hebei Education Department, China (Grant No. QN2017135).

†Corresponding author. E-mail: xqiao77@163.com

© 2017 Chinese Physical Society and IOP Publishing Ltd

tovoltaic properties of solar cells. The influence mechanisms that interface states, conduction band offset, and front contact impact on the carrier transport, interface recombination and cell performance were studied in detail. Finally, by optimizing D_{it}, ΔE_c, and W_{TCO}, the p-type a-SiC:H(n)/c-Si(p) SHJ solar cell with efficiency of 23.06% was achieved.

2. Modeling

2.1. Physical model

The SHJ solar cell structure TCO/a-SiC:H(n)/c-Si(p)(textured)/a-Si:H(i)/a-Si:H(p)/TCO was modeled by AFORS-HET. Within the bulk of each layer, AFORS-HET solves one-dimensional Poisson equation and the electron and hole continuity equations for a given defect state distribution using Shockley–Read–Hall recombination statistics,[12,13]

$$-\frac{\varepsilon_0\varepsilon_r}{q}\frac{\partial^2\varphi(x,t)}{\partial x^2} = p(x,t)-n(x,t)+N_D-N_A+\sum_{\text{defects}}\rho_t(x,t), \quad (1)$$

$$-\frac{1}{q}\frac{\partial j_n(x,t)}{\partial x} = G_n(x,t)-R_n(x,t)-\frac{\partial}{\partial t}n(x,t), \quad (2)$$

$$\frac{1}{q}\frac{\partial j_p(x,t)}{\partial x} = G_p(x,t)-R_p(x,t)-\frac{\partial}{\partial t}p(x,t), \quad (3)$$

where φ, q, ρ_t, and n/p are the electric potential, electron charge, defect density of charged defects, and electron/hole density, respectively. $j_{n/p}$ and $N_{D/A}$ denote the electron/hole current and the donor/acceptor concentration. $G_{n/p}$ and $R_{n/p}$ represent the electron/hole optical generation rate and recombination rate, respectively.

For amorphous layers, it has been assumed that there are both exponential band tail states and Gaussian mid-gap states (associated to silicon dangling bonds) in the bandgap. The valence and conduction band tail states are usually given as follows

$$g_A(E) = G_{AO}\exp\left[\frac{E-E_c}{E_A}\right], \quad (4)$$

$$g_D(E) = G_{DO}\exp\left[\frac{E_v-E}{E_D}\right], \quad (5)$$

where $G_{AO}(E)$ and $G_{DO}(E)$ are the densities per energy range for tail states at the band edge energies E_V and E_C. E_A and E_D stand for characteristic parameters for the conduction and valence band tail states, respectively.

The mid-gap states are described by Gaussian distributions of acceptor-like states and donor-like states,i.e.

$$g_A(E) = N_{AG}\exp\left\{-\frac{1}{2}\left[\frac{(E-E_A^{db})^2}{\sigma_A^2}\right]\right\}, \quad (6)$$

$$g_D(E) = G_{DG}\exp\left\{-\frac{1}{2}\left[\frac{(E-E_D^{db})^2}{\sigma_D^2}\right]\right\}, \quad (7)$$

where E_A^{db} and E_D^{db} are the peak energy position. N_{AG} and N_{DG} denote the effective density of states. σ_A and σ_D represent the standard energy deviation of the Gaussian acceptor and donor levels, respectively.

Furthermore, the voltaged controlled boundary condition is selected, and the potential at the front contact ($x=0$) is fixed at zero. Then at the front contact ($x=0$), the boundary condition is

$$\varphi(0) = 0, \quad (8)$$

$$J_n(0) = q\cdot S_n^f(n(0)-n_{eq}(0)), \quad (9)$$

$$J_p(0) = -q\cdot S_p^f(p(0)-p_{eq}(0)). \quad (10)$$

Accordingly, the boundary condition at the back contact($x=L$) is

$$\varphi(L) = \phi_f-\phi_b+V, \quad (11)$$

$$J_n(L) = -q\cdot S_n^b(n(L)-n_{eq}(L)), \quad (12)$$

$$J_p(L) = +q\cdot S_p^b(p(L)-p_{eq}(L)), \quad (13)$$

where ϕ and S are the metal work function and surface recombination velocity, respectively.

Table 1. Basic parameters adopted for layers used in the simulation.

Parameters	n-a-SiC:H	i-a-Si:H	p-c-Si	p-a-Si:H
Layer thickness/nm	10	5	3×10^5	5
Dielectric constant	9.7	11.9	11.9	11.9
Electron affinity/eV	variable	3.9	4.05	3.9
Optical band gap/eV	1.96	1.72	1.12	1.72
Effective conduction band density/cm^{-3}	1×10^{20}	1×10^{20}	2.8×10^{19}	1×10^{20}
Effective valence band density/cm^{-3}	1×10^{20}	1×10^{20}	1.04×10^{19}	1×10^{20}
Electron mobility/cm$^2\cdot$V$^{-1}\cdot$s^{-1}	10	20	1046	15
Hole mobility/cm$^2\cdot$V$^{-1}\cdot$s^{-1}	1	5	413.8	5
Doping concentration of acceptors/cm^{-3}	0	0	1.46×10^{16}	9×10^{19}
Doping concentration of donors/cm^{-3}	variable	0	0	0
Tail defect density/cm$^{-3}\cdot$eV^{-1}	2×10^{21}	2×10^{21}		2×10^{21}
Gaussian defect density/cm^{-3}	6.9×10^{19}	5×10^{15}	1×10^{11}	6.9×10^{19}
Layer density/g$\cdot$cm^3	2.328	2.328	2.328	2.328
Auger recombination coefficient for electron/cm$^6\cdot$s^{-1}	0	0	2.2×10^{-31}	0
Auger recombination coefficient for hole/cm$^6\cdot$s^{-1}	0	0	9.9×10^{-32}	0

2.2. Input parameters for simulation

The basic parameters for the modeled structure TCO/a-SiC:H(n)/c-Si(p) (textured)/a-Si:H(i)/a-Si:H(p)/TCO are listed in Table 1. The gap state densities of all kinds of amorphous layers were taken from Refs. [14] and [15]. Figure 1 shows the gap state distribution in the a-SiC:H(n) and a-Si:H(p) layers. The energy difference between the donor-type and acceptor-type defect is 0.3 eV. As for the a-Si:H(i) layer, the acceptor-like and donor-like defect are symmetrically positioned 0.15 eV from the midgap with a much lower density(not shown). The interface defects density at the front a-SiC:H(n)/c-Si(p) interface was modeled by an additional defect rich layer 5-nm thick. Then the volume defect density range of 2×10^{15} cm^{-3}·eV^{-1}–2×10^{19} cm^{-3}·eV^{-1} in the 5-nm thick layer corresponds to the surface defect density range of 1×10^{9} cm^{-3}·eV^{-1}–1×10^{13} cm^{-3}·eV^{-1}. The recombination velocities at the front and back contact were both fixed at 1×10^{7} cm/s. The operation temperature was set at 300 K, and the solar illumination was set at AM 1.5 (a power density of 100 mW/cm^2). The light reflection of the front and the back contacts was set at 0.1 and 1, respectively. Moreover, in Subsections 3.1 and 3.2, the influence of TCO/a-SiC:H(n) front contact was ignored by setting the front contact as an ohmic contact.

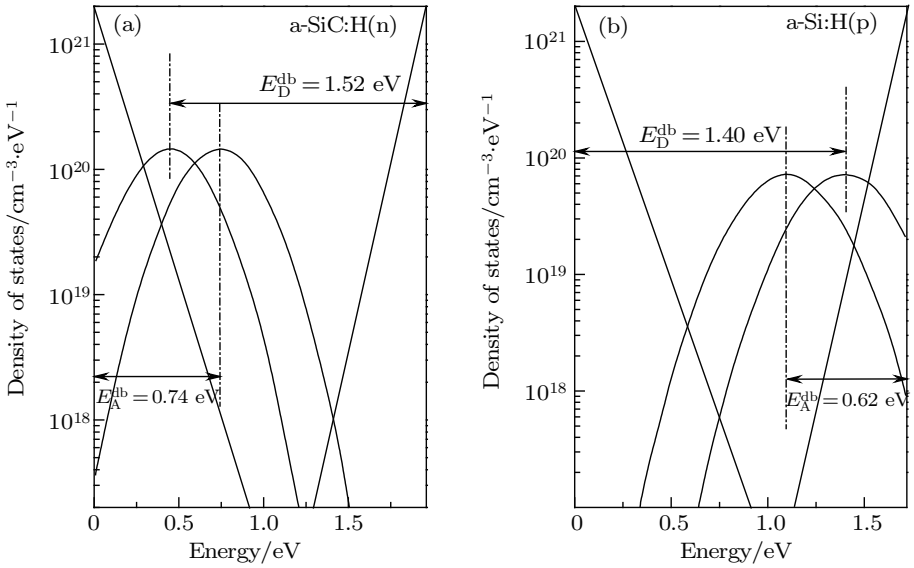


Fig. 1. The gap state distribution in the (a) a-SiC:H(n) and (b) a-Si:H(p) layers in the simulations.

3. Results and discussion

3.1. Influence of interface states

Figure 2 shows the calculated *J*–*V* characteristics of the a-SiC:H(n)/c-Si(p) cells with different interface state densities. It can be seen that the increase of D_{it} leads directly to a loss in V_{oc}. When the D_{it} is above 1×10^{11} cm^{-2}·eV^{-1}, V_{oc} drops sharply. This result is in agreement with the Refs. [14], [16]–[18]. The influence of the interface states on V_{oc} can be described by the following formula proposed by Jensen *et al.*[19]

$$V_{oc}=\frac{1}{q}\left\{\Phi_c-AkT\ln\left(\frac{qN_vS_{it}}{j_{sc}}\right)\right\}, \tag{14}$$

where Φ_c and S_{it} denote the effective barrier height in c-Si and interface recombination velocity, respectively. Obviously, a high D_{it} means a high S_{it} at the a-SiC:H(n)/c-Si(p) interface. It can be seen from Eq. (14) that the increase of S_{it} leads to a logarithmic decrease in V_{oc}.

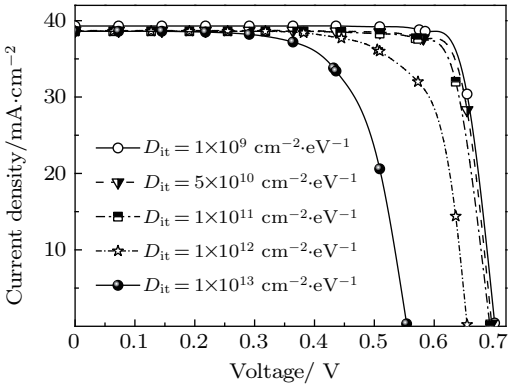


Fig. 2. The calculated *J*–*V* characteristics of the a-SiC:H(n)/c-Si(p) SHJ solar cells with different interface states' densities.

To further understand the sensitivity of V_{oc} to the interface states, we calculated the electric field distribution in the a-SiC:H(n)/c-Si(p) heterojunction for the two cases of low $D_{it}=1\times10^{10}$ cm^{-2}·eV^{-1} and high $D_{it}=5\times10^{12}$ cm^{-2}·eV^{-1}, as shown in Fig. 3(a). It can be seen that the interface with high D_{it} has a very strong electric field at the a-SiC:H(n)/c-Si(p) interface but a weak field on the c-Si(p) side. This can be attributed to the high density of interface states that can trap most of the electrons during the p-n junction formation.

When an n-type a-SiC:H layer is in contact with a p-type c-Si wafer, electrons will flow from the n-side to the p-side to equilibrate their Fermi levels. In the high interface state density case, most electrons will be trapped in the states. These occupied acceptor-like interface states will become a high density of negative space charges on the c-Si(p) surface, leading to a localized space charge region on the c-Si(p) side. As a result, a very high electric field at the interface and a collapsed one on the c-Si(p) side come into being. Furthermore, figure 3(b) indicates that for the high D_{it} case, the band bending on the c-Si(p) wafer side is flattened. This increases the interface recombination velocity, giving rise to a striking fall in V_{oc}. Therefore, in order to obtain high V_{oc}, it is very critical to ensure a good surface passivation for SHJ solar cells. The interface states' density should be controlled below 1×10^{11} cm^{-2}·eV^{-1}.

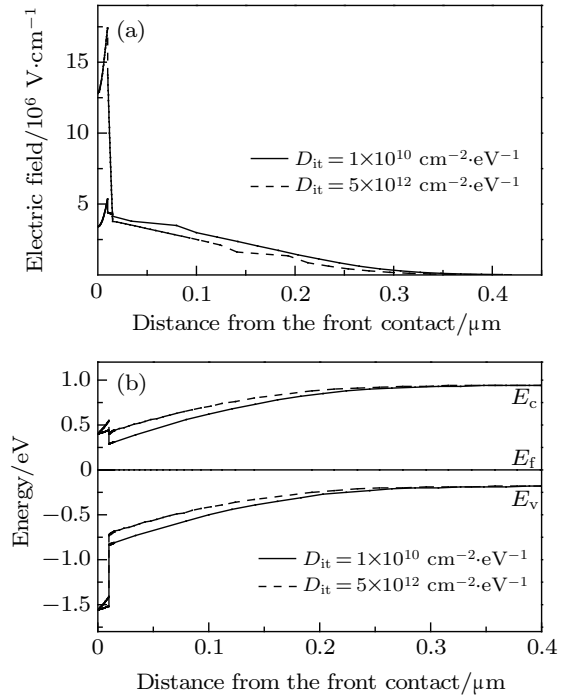


Fig. 3. The (a) electric field and (b) equilibrium energy band of the a-SiC:H(n)/c-Si(p) SHJ solar cells for the cases with $D_{it} = 1 \times 10^{10}$ cm^{-2}·eV^{-1} and $D_{it} = 5 \times 10^{12}$ cm^{-2}·eV^{-1}.

Figure 4 shows the dependence of J_{sc} and V_{oc} on the interface states density for the a-SiC:H(n) emitter and a-Si:H emitter, respectively. It can be seen that both J_{sc} and V_{oc} show the same varying trend with the increase of D_{it} for the two emitters. What is more, much higher J_{sc} was obtained in the a-SiC:H(n)/c-Si(p) structures. We attributed this to the larger bandgap of a-SiC:H(n), which decreases optical absorption losses in the layer. Figure 5 shows the IQE curves for the a-SiC:H(n)/c-Si(p) and a-Si:H(n)/c-Si(p) structures. It clearly shows that the a-SiC:H(n)/c-Si(p) structure has a higher blue response than the a-Si:H(n)/c-Si(p) structure. This means that there are more holes generated in the a-SiC:H(n) layer that are able to pass the junction and then to enhance the short circuit current density.

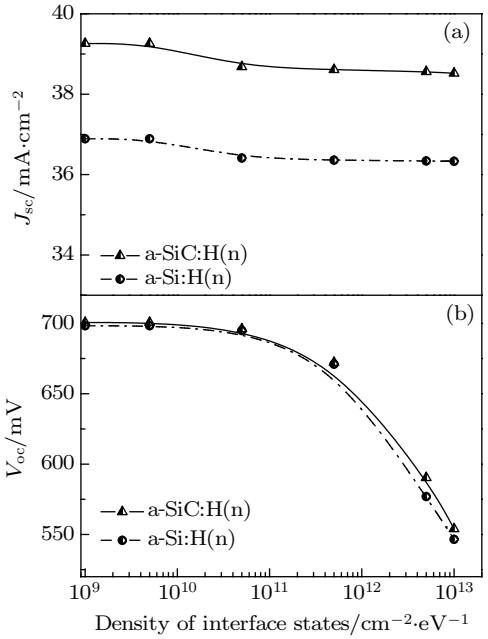


Fig. 4. The (a) J_{sc} and (b) V_{oc} of SHJ solar cells with different interface state densities for the a-SiC:H(n) emitter and a-Si:H(n) emitter.

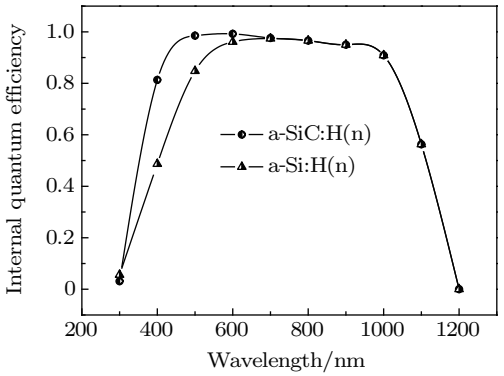


Fig. 5. Internal quantum efficiency (IQE) of the a-SiC:H(n)/c-Si(p) and the a-Si:H(n)/c-Si(p) SHJ solar cells.

3.2. Influence of the conduction band offset

Compared to a-Si:H(n), the a-SiC:H(n) emitter with a larger bandgap may give rise to a higher conduction band offset (ΔE_c) at the a-SiC:H/c-Si interface. Considering the ΔE_c can vary with the deposition conditions, it is essential to carefully inspect the impacts of ΔE_c on the performance of solar cells.[20,21]

Figure 6 shows the simulated dependence of the solar cell performance on the conduction band offset. Here, two cases of the interface defect density, $D_{it} = 5 \times 10^{11}$ cm^{-2}·eV^{-1} and $D_{it} = 1 \times 10^{12}$ cm^{-2}·eV^{-1}, were assumed. Simulation reveals that the open circuit voltage and fill factor are very sensitive to ΔE_c. Moreover, V_{oc} is relatively high when ΔE_c falls in the range of 0.15 eV∼0.2 eV. On the other hand, FF is in a low level when ΔE_c is above 0.15 eV. It can be clearly

understood through the equilibrium energy band diagram for the a-SiC:H(n)/c-Si(p) heterojunction with different conduction band offsets, as shown in Fig. 7(a). It can be seen that with the increase of ΔE_c, the band bending in the c-Si absorber is enhanced. As shown in Fig. 7(a), the built-in voltage is enhanced from 530 mV to 700 mV as ΔE_c increases from 0.05 eV to 0.25 eV. This leads to a strong inversion layer forming at the a-SiC:H(n)/c-Si(p) interface. Then the interface recombination is suppressed due to fewer majority carrier holes available there for recombination.

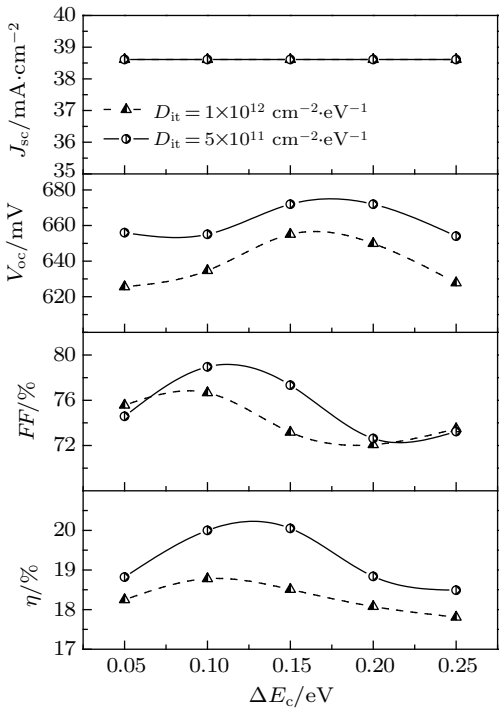


Fig. 6. The simulated performance of the a-SiC:H(n)/c-Si(p) solar cell as a function of ΔE_c, for the cases with $D_{it} = 5 \times 10^{11}$ cm^{-2}·eV^{-1} and $D_{it} = 1 \times 10^{12}$ cm^{-2}·eV^{-1}.

Figure 7(b) illustrates the simulated electric field distribution at the a-SiC:H(n)/c-Si(p) heterojunction. As can be seen from Fig. 7(b), the higher ΔE_c results in a stronger electric field at both the a-SiC:H(n) and c-Si(p) sides. This further suppresses the interface recombination, leading to an increase in the V_{oc}. However, when ΔE_c is above 0.2 eV, the enhanced band offset gives rise to a transport barrier for electrons. Hence, electrons will accumulate at the a-SiC:H(n)/c-Si(p) interface. This not only causes electrons trapped in the acceptor interface states, but also encourages the holes in the absorber c-Si(p) to back diffuse and recombine with electrons. All this offsets the suppressing effect of the inversion layer on the interface recombination. The net result is that V_{oc} and FF strongly decrease when ΔE_c is in the range of 0.20 eV∼0.25 eV. Therefore, higher efficiency can be obtained in the a-SiC:H/c-Si SHJ solar cells with ΔE_c in the range of 0.10 eV∼0.15 eV.

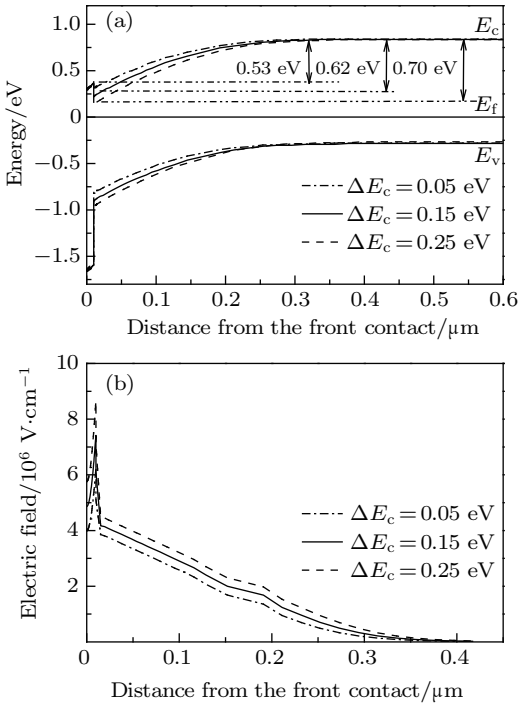


Fig. 7. The (a) simulated equilibrium energy band diagram and (b) electric field distribution of the front a-SiC:H(n)/c-Si(p) heterojunction with different conduction band offsets.

3.3. Influence of TCO/a-SiC:H(n) front contact

The work function of transparent conductive oxide (W_{TCO}) is usually higher than that of a-SiC:H(n) layer. Therefore, when TCO and a-SiC:H(n) are brought into contact, a Schottky barrier develops at the TCO/a-SiC:H(n) interface, which significantly influences the performance of SHJ solar cells.

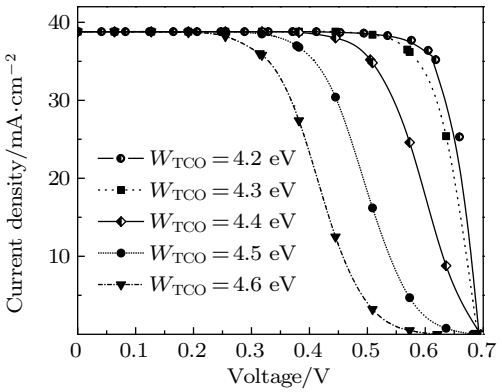


Fig. 8. The calculated J–V characteristics of the a-SiC:H(n)/c-Si(p) cells with different work functions of transparent conductive oxide (W_{TCO}), where $D_{it} = 1 \times 10^{11}$ cm^{-2}·eV^{-1}, $\Delta E_c = 0.15$ eV, and $N_d^{a-SiC:H(n)} = 7.09 \times 10^{19}$ cm^{-3} were assumed.

Figure 8 shows the J–V characteristics of the a-SiC:H(n)/c-Si(p) cells with different values of W_{TCO}. The doping concentration of a-SiC:H(n) ($N_d^{a-SiC:H(n)}$) was set as 7.09×10^{19} cm^{-3}, corresponding to the $W_{a-SiC:H(n)} = 4.2$ eV. The values of D_{it} and ΔE_c were fixed at 1×10^{11} cm^{-2}·eV^{-1} and 0.15 eV, respectively. It can be seen that V_{oc} and FF are strongly influenced by the W_{TCO}. When the W_{TCO} is higher

than 4.3 eV, V_{oc} and FF decrease considerably. What is more, the S-shaped J–V curves can be clearly observed when $W_{TCO} \geq 4.5$ eV. Similar results were also reported by Zhao *et al.* and Dao *et al.*[16,17]

Figure 9 shows the equilibrium energy band diagram of the a-SiC:H(n)/c-Si(p) cells for the two cases of $W_{TCO} = 4.2$ eV and $W_{TCO} = 4.6$ eV. As shown in Fig. 9, when W_{TCO} is 4.2 eV, the TCO/a-SiC:H(n) front contact is in flat band condition. However, when W_{TCO} is high, the conduction band near the TCO/a-SiC:H(n) interface distinctly bends upward, forming an inverted junction to the a-SiC:H(n)/c-Si(p) junction. Consequently, the Schottky front contact with high W_{TCO} severely hinders the electron transport by forming a resistive bed. This induces the generation of S-shaped J–V curves. Furthermore, for the case of $W_{TCO} = 4.6$ eV, the Fermi level has an obvious shift towards the valence band, and meanwhile a strongly flattened band bending occurs on the absorber side. This is mainly because when W_{TCO} is 4.6 eV, the built-in potential V_D in the TCO/a-SiC:H(n) Schottky contact is as high as 0.4 eV. The high V_D not only drives the thin a-SiC:H(n) emitter layer into depletion but also, more importantly, additional electrons in the absorber have to be used to shield the electric field. As a result, the width of the space charge region and the band bending on the absorber side are drastically reduced.

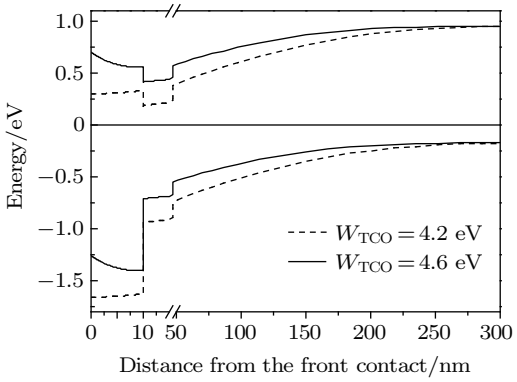


Fig. 9. The band diagram of the a-SiC:H(n)/c-Si(p) cell for the cases with $W_{TCO} = 4.2$ eV and $W_{TCO} = 4.6$ eV, where the $D_{it} = 1 \times 10^{11}$ cm^{-2}·eV^{-1}, $\Delta E_c = 0.15$ eV, and $N_d^{a-SiC:H(n)} = 7.09 \times 10^{19}$ cm^{-3} were assumed.

Figure 10 indicates that the flattened band bending in the case of high $W_{TCO} = 4.6$ eV results in a significantly weakened electric field on the c-Si(p) side. This enhances the interface recombination, leading to a sharp decrease in both V_{oc} and FF. So it is necessary to carefully tune the value of W_{TCO} to obtain high efficiency a-SiC:H(n)/c-Si(p) solar cells. Also, our simulation results show that the influence of the TCO/a-SiC:H(n) front contact is negligible when the V_D in the front contact TCO/a-SiC:H(n) is no higher than 0.2 eV. This means that W_{TCO} should be as low as possible for the p-type SHJ solar cells.

Finally, according to the analyses and optimum parameters provided above, we modeled the J–V characteristics for the a-SiC:H(n)/ c-Si(p) SHJ solar cell by choosing W_{TCO} as 4.2 eV, D_{it} as 1×10^{10} cm^{-2}·eV^{-1} and ΔE_c as 0.15 eV. As we expected, high performance with $V_{oc} = 721.5$ mV, $J_{sc} = 39.26$ mA·cm^{-2}, $FF = 0.814$, and $\eta = 23.06\%$ was achieved. For p-type SHJ solar cell the improved efficiency is 1.7 points over the record efficiency by experiment. However, it is still lower than the best efficiency achieved on n-type SHJ solar cell. This is mainly due to the different energy band structure between the p-type and n-type SHJ solar cells. N-type SHJ solar cell has the higher minority carrier band offset at the interface, which can suppress the interface recombination effectively. On the other hand, the efficiency of p-type SHJ solar cell can be further improved by optimizing its back c-Si(p)/a-Si:H(p+)/TCO structure.[22] The related research is right going on.

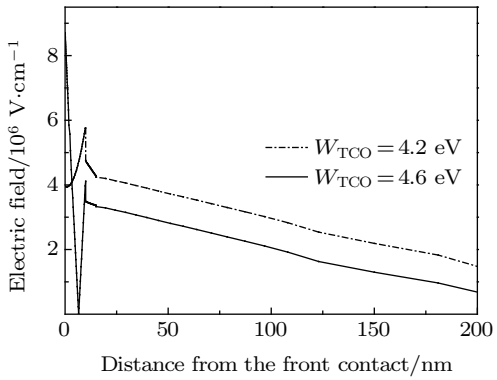


Fig. 10. The electric field of the a-SiC:H(n)/c-Si(p) cell for the cases $W_{TCO} = 4.2$ eV and $W_{TCO} = 4.6$ eV, where the $D_{it} = 1 \times 10^{11}$ cm^{-2}·eV^{-1}, $\Delta E_c = 0.15$ eV, and $N_d^{a-SiC:H(n)} = 7.09 \times 10^{19}$ cm^{-3} were assumed.

4. Conclusions

In summary, by numerical computer modeling we have simulated the p-type SHJ solar cells with the structure of TCO/a-SiC:H(n)/c-Si(p) (textured)/a-Si:H(i)/a-Si:H(p+)/TCO. The influence of interface states, conduction band offset, and front contact on the performance of the p-type SHJ solar cells was studied in detail. It is shown that by using wide bandgap a-SiC:H(n) instead of a-Si:H(n) as the window layer, the short-circuit current can be remarkably increased. What is more, the open circuit voltage and fill factor are very sensitive to the interface states, conduction band offset and work function of TCO. Firstly, a poor a-SiC:H(n)/c-Si(p) interface with high D_{it} can result in a striking fall in the open circuit voltage due to a flattened band bending on the c-Si(p) wafer side. In order to achieve high V_{oc} the interface state density should be lower than 1×10^{11} cm^{-2}·eV^{-1}. Secondly, the increase of conduction band offset may induce a strong inversion layer forming at the a-SiC:H(n)/c-Si(p) interface, which

suppresses the surface recombination. On the other hand, it gives rise to a transport barrier for electrons, which enhances carrier recombination due to electrons accumulation at the interface. The trade-off between the inversion layer and transport barrier leads to the ΔE_c in the range of 0.1 eV–0.15 eV. Thirdly, the W_{TCO} should be as low as possible. It is shown that when the W_{TCO} is high, it can drive the J–V curves into an S-shape, owing to an inverted junction forming at the front contact. Meanwhile, high W_{TCO} can also reduce V_{oc} and FF drastically due to the enhanced interface recombination. Finally, by employing the optimum parameters for D_{it}, W_{TCO}, and ΔE_c, the p-type a-SiC:H(n)/c-Si(p) SHJ solar cell with the high efficiency of 23.06% was achieved.

References

[1] Tanaka M, Taguchi M, Matsuyama T, Sawada T, Tsuda S, Nakano S, Hanafusa H and Kuwano Y 1992 *Jpn. J. Appl. Phys.* **31** 3518

[2] Masuko K, Shigematsu M, Hashiguchi T, Fujishima D, Kai M, Yoshimura N, Yamaguchi T, Ichihashi Y, Mishima T, Matsubara N, Yamanishi T, Takahama T, Taguchi M, Maruyama E and Okamoto S 2014 *IEEE J. Photovoltaics* **4** 1433

[3] Schmidt M, Korte L, Laades A, Stangl R, Schubert C Angermann H, Conrad E and Maydell K 2007 *Thin Solid Films* **515** 7475

[4] Pysch D, Bivour M, Hermle M and Glunz S 2011 *Thin Solid Films* **519** 2550

[5] Descoeudres A, Holman ZC, Barraud L, Morel S, De Wolf S and Ballif C 2013 *IEEE J. Photovoltaics* **3** 83

[6] Wang Q, Page M, Iwaniczko E, Xu Y, Roybal L, Bauer R, To B, Yuan H, Duda A and Hasoon F 2010 *Appl. Surf. Sci.* **96** 013507

[7] Korte L, Conrad E, Angermann H, Stangl R and Schmidt M 2009 *Sol. Energy Mater. Sol. Cells* **93** 905

[8] Pysch D, Ziegler J, Becker J P, Suwito D, Janz S, Glunz S W and Hermle M 2009 *Appl. Phys. Lett.* **94** 093510

[9] Mao H, Wuu D, Wu B, Lo S, Hsieh H and Horng R 2012 *Thin Solid Films* **520** 2110

[10] Miyajima S, Irikawa J, Yamada A and M Konagai 2010 *Appl. Phys. Lett.* **97** 023504

[11] Mueller T, Duengen W, Ma Y, Job R, Scherff M and Fahrner W 2007 *J. Appl. Phys.* **102** 074505

[12] Stangl R, Kriegel M, and Schmidt M 2006 *World Conference on Photovoltaic Energy Conversion*, May 7–12, 2006, Hawaii, USA, Vol. 2, p. 1350

[13] Froitzheim A, Stangl R, Elstner L, Schmidt M, and Fuhs W 2002 *Conference Record of the* 29*th IEEE Photovoltaic Specialists Conference*, May 19–24, 2002, New Orleans, USA, p. 1238

[14] Stangl R, Froitzheim A, Schmidt M, and Fuhs W 2003 *Proceedings of the Third World Conference on Photovoltaic Energy Conversion*, May 7–12, 2003, Osaka, Japan, p. 1005

[15] Kanevce A and Metzger W 2009 *J. Appl. Phys.* **105** 094507

[16] Zhao L, Zhou C, Li H, Diao H and Wang W 2008 *Sol. Energy Mater. Sol. Cells* **92** 673

[17] Dao V, Heo J, Choi H, Kim Y, Park S, Jung S, Lakshminarayan N and Yi J 2010 *Sol. Energy* **84** 777

[18] Zhou J, Di M, Sun T, Sun Y and Wang H 2010 *Acta Phys. Sin.* **59** 8870 (in Chinese)

[19] Jensen N, Hausner R, Bergmann R, Werner J and Rau U 2002 *Progress in Photovoltaics: Research and Applications* **10** 1

[20] Essick J and Cohen J 1989 *Appl. Phys. Lett.* **55** 1232

[21] Nath M, Chatterjee P, Damon-Lacoste J and Cabarrocas P 2008 *J. Appl. Phys.* **103** 034506

[22] Zhao L, Zhou C, Li H, Diao H and Wang W 2008 *Acta Phys. Sin.* **57** 3212 (in Chinese)